

Molecular Characterization of Oxysterol Binding to the Epstein-Barr Virus-induced Gene 2 (GPR183)*[‡]

Received for publication, June 3, 2012. Published, JBC Papers in Press, August 8, 2012, DOI 10.1074/jbc.M112.387894

Tau Benned-Jensen[‡], Christoffer Norn[§], Stephane Laurent[¶], Christian M. Madsen[‡], Hjalte M. Larsen[§], Kristine N. Arfelt[‡], Romain M. Wolf[¶], Thomas Frimurer^{§**}, Andreas W. Sailer[¶], and Mette M. Rosenkilde^{‡1}

From the [‡]Laboratory for Molecular Pharmacology, Department of Neuroscience and Pharmacology, Faculty of Health and Medical Sciences, University of Copenhagen, Blegdamsvej 3, DK-2200 Copenhagen N, Denmark, the [§]Novo Nordisk Foundation Center for Protein Research, Faculty of Health and Medical Sciences, University of Copenhagen, Blegdamsvej 3, DK-2200 Copenhagen N, Denmark, the [¶]Developmental and Molecular Pathways, Novartis Institutes for BioMedical Research, 4056 Basel, Switzerland, the [¶]Global Discovery Chemistry, Novartis Institutes for BioMedical Research, 4056 Basel, Switzerland, and the ^{**}Novo Nordisk Foundation Center for Basic Metabolic Research, Faculty of Health and Medical Sciences, University of Copenhagen, Blegdamsvej 3, DK-2200 Copenhagen N, Denmark

Background: EBI2 was recently deorphanized as the first oxysterol-activated receptor, but the binding mode remains unknown.

Results: Mutational analysis showed that substitution of Arg-87, Tyr-112, Tyr-116, and Tyr-260 abolished agonist binding and EBI2 activation.

Conclusion: Oxysterol binding is dependent on residues in TM-II, -III, and -VI.

Significance: This is the first study to examine the binding mode of these novel 7TM receptor agonists.

Oxysterols are oxygenated cholesterol derivatives that are emerging as a physiologically important group of molecules. Although they regulate a range of cellular processes, only few oxysterol-binding effector proteins have been identified, and the knowledge of their binding mode is limited. Recently, the family of G protein-coupled seven transmembrane-spanning receptors (7TM receptors) was added to this group. Specifically, the Epstein-Barr virus-induced gene 2 (EBI2 or GPR183) was shown to be activated by several oxysterols, most potently by 7 α ,25-dihydroxycholesterol (7 α ,25-OHC). Nothing is known about the binding mode, however. Using mutational analysis, we identify here four key residues for 7 α ,25-OHC binding: Arg-87 in TM-II (position II:20/2.60), Tyr-112 and Tyr-116 (positions III:09/3.33 and III:13/3.37) in TM-III, and Tyr-260 in TM-VI (position VI:16/6.51). Substituting these residues with Ala and/or Phe results in a severe decrease in agonist binding and receptor activation. Docking simulations suggest that Tyr-116 interacts with the 3 β -OH group in the agonist, Tyr-260 with the 7 α -OH group, and Arg-87, either directly or indirectly, with the 25-OH group, although nearby residues likely also contribute. In addition, Tyr-112 is involved in 7 α ,25-OHC binding but via hydrophobic interactions. Finally, we show that II:20/2.60 constitutes an important residue for ligand binding in receptors carrying a positively charged residue at this position. This group is dominated by lipid- and nucleotide-activated receptors, here exemplified by the CysLTs, P2Y12, and P2Y14. In conclusion, we present the first molecular characterization of oxysterol binding to a 7TM receptor and identify position II:20/2.60 as a generally important residue for ligand binding in certain 7TM receptors.

Oxysterols encompass a group of oxygenated cholesterol derivatives that are synthesized by enzymatic and nonenzymatic mechanisms in various organs. These molecules play an important role in a range of cellular processes, including inflammation (1), lipid metabolism (2), and apoptosis (3). The molecular targets of oxysterols are only starting to emerge and many remain enigmatic. Given their hydrophobic nature, these molecules are able to modulate the activity of cellular effectors either directly by binding or indirectly by changing the physicochemical properties of the plasma membrane upon incorporation (4). Interestingly, two distinct receptor families are represented among the few effectors that are known to bind oxysterols, namely the nuclear receptor transcription factors and the G protein-coupled seven transmembrane (7TM)² receptors. Members of the former group include the liver X receptor α and β isoforms, both of which are activated by several oxysterols such as 22(R)-hydroxycholesterol and 24(S)-hydroxycholesterol (5–7). In addition, another nuclear receptor, the retinoic acid-related orphan receptor γ , was recently suggested to be activated by various oxysterols (8). Of note, this receptor is important for T_H17 cell differentiation and T_H17 cell-mediated autoimmune disease (9, 10) suggesting a prominent role for oxysterol-induced nuclear receptor activity in both physiological and pathophysiological settings.

Recently, the family of 7TM receptors was discovered to be oxysterols targets when two oxysterol-activated receptors were identified. These are smoothened, an essential element of the hedgehog signaling pathway (11), and the Epstein-Barr virus-

* S. L., R. W., and A. W. S. are employees of Novartis Pharma AG and hold stock or stock options in the company.

⌘ Author's Choice—Final version full access.

[‡]This article contains supplemental Fig. 1.

¹ To whom correspondence should be addressed. Tel.: + or 00 45-30604608; Fax: + or 00 45-35327610; E-mail: rosenkilde@sund.ku.dk.

² The abbreviations used are: 7TM, seven transmembrane; 7 α ,25-OHC, 7 α ,25-dihydroxycholesterol; CREB, cAMP-response element-binding protein; CysL Ts, cysteinyl leukotriene receptors 1 and 2; hEBI2, human EBI2; Pro11:18 receptor: receptor in which the conserved TM-II Pro is found at position II:18/2.58; Pro11:19 receptor: receptor in which the conserved TM-II Pro is found at position II:19/2.59; TM, transmembrane; GTP γ S, guanosine 5'-3'-O-(thio)triphosphate; CysLT, cysteinyl leukotriene; hEBI2, human EBI2; LT, leukotriene; SPA, scintillation proximity assay.

induced receptor 2 (EBI2) also known as GPR183 (12, 13). EBI2, the focus of this study, belongs to the rhodopsin-like subfamily of 7TM receptors and is expressed primarily in lymphoid tissues and leukocytes (14, 15). Prior to its orphanization, a characterization of this receptor's apparent constitutive activity revealed that it signals through G α_i (14). Biologically, EBI2 was later shown to play an important role in humoral immune responses by regulating B cell trafficking within lymphoid follicles (16, 17). Specifically, activated B cells residing in the germinal centers down-regulate the expression of EBI2 and, upon translocating to the inter/outer follicular areas, up-regulate the level of EBI2 suggesting that the receptor functions as a chemotactic receptor by responding to an (at the time) unidentified agonist. This agonist was finally identified as the oxysterol 7 α ,25-OHC, which binds EBI2 with high affinity and selectivity (12, 13). Activation of EBI2 by 7 α ,25-OHC leads to G α_i activation and ultimately triggers migration of EBI2-expressing leukocytes *ex vivo* and *in vivo* (12, 13). Importantly, activated B cells that are deficient in either CH25H (the enzyme that catalyzes the hydroxylation at the 25-position) (12) or EBI2 (16, 17) are unable to migrate to the outer region of the germinal center. Ultimately, this results in a significantly reduced number of plasma cells thus underscoring the biological importance of this novel agonist-receptor pair.

Whereas structural data regarding the binding mode of oxysterols to nuclear receptors (8) and the oxysterol-binding protein (18) exist, the binding mode of oxysterols to 7TM receptors is unknown. However, pharmacophore studies on the 7 α - and 25-OH groups in the EBI2 agonist suggest that both are tightly involved in ligand binding as even subtle changes in hydroxyl position result in a significant decrease in affinity, suggesting that a clearly defined set of anchor residues are present in EBI2 (12, 13). Here, we have used mutational analysis to identify these residues, and *in silico* docking simulations to explore the possible binding modes of 7 α ,25-OHC. The important residues include an Arg in the top of TM-II (Arg-87 at position II:20/2.60),³ a Tyr in TM-III (Tyr-116 at position III:13/3.37) and a Tyr in TM-VI (Tyr-260 at position VI:16/6.51). Furthermore, the Tyr at position III:09/3.33 (Tyr-112) also play a prominent role in agonist binding. We also show that Arg or Lys residues at position II:20/2.60 are highly important for ligand binding in other 7TM receptors, here exemplified by the cysteinyl leukotriene receptors 1 and 2 (CysLTs) and two P2Y receptors (P2Y12 and P2Y14). Finally, as we previously have identified the Arg at position II:20/2.60 as a major regulator of EBI2 constitutive activity (19), our results also indicate that the majority of this activity likely has been a result of agonist contamination as reported for other lipid-activated receptors as well (20).

EXPERIMENTAL PROCEDURES

Materials—The cDNA encoding human EBI2 was from an in-house library, and cDNAs encoding CysLT1, CysLT2, P2Y12, and P2Y14 were bought from Missouri S&T cDNA Resource Center. The promiscuous chimeric G protein

G $_{qi}$ 4myr was kindly provided by Evi Kostenis (Rheinische Friedrich-Wilhelm University, Bonn, Germany). LipofectamineTM 2000 reagent and Opti-MEM was purchased from Invitrogen, and FuGENE 6 reagent was from Roche Applied Science. The PathHunter β -arrestin kit was from DiscoverX. SteadyLite (lyophilized substrate solution) was from Perkin-Elmer Life Sciences, and 3,3',5,5'-tetramethylbenzidine substrate was purchased from KemEnTech. Goat anti-mouse horseradish peroxidase-conjugated antibody was from Pierce, and mouse anti-M1-FLAG antibody, sodium lactate, UDP-galactose, and ADP were from Sigma. [³⁵S]GTP γ S was from PerkinElmer Life Sciences, and [³H]7 α ,25-OHC was custom-synthesized (Tritec) and repurified periodically at Novartis. All oxysterols were purchased from Avanti Polar Lipids and dissolved in pure DMSO. The cysteinyl leukotrienes LTD₄ and LTC₄ were from Cayman Chemicals.

Receptor Constructs—Constructs used in GTP γ S, β -arrestin recruitment, and competition binding studies carried an N-terminal M1-FLAG tag as described previously (19). Site-directed mutagenesis was carried out using the QuikChange protocol and *Pfu* polymerase (Stratagene). All mutations were verified by DNA sequencing.

Tissue Culture and Transfections—HEK293 cells were grown in DMEM (Invitrogen) adjusted to contain 4500 mg/liter glucose, 10% FBS (fetal bovine serum), 180 units/ml penicillin, and 45 μ g/ml penicillin/streptomycin at 10% CO₂. Stably transfected CHO FLP-IN cells were grown in Ham's F-12 containing 10% FBS, 1% glutamine, penicillin/streptomycin, and hygromycin (500 μ g/ml) at 5% CO₂. Stably transfected CHO K1.A2 cells used in β -arrestin assays were grown in Ham's F-12 containing 10% FBS, 1% glutamine, penicillin/streptomycin, and hygromycin (250 μ g/ml) at 5% CO₂. CHO cells stably expressing G $_{qi5}$ and EBI2 mutants were maintained in growth medium (DMEM/Ham's F-12) supplemented with 10% heat-inactivated fetal calf serum and selection markers (0.25 mg/ml Zeocin, 5 μ g/ml puromycin, and 0.4 mg/ml G418). For membrane preparations, transient transfections were performed using the calcium precipitation method, and FuGENE 6 and Lipofectamine 2000 were used in β -arrestin assays and for generation of stable CHO FLP-IN clones, respectively.

Membrane Preparation—Membranes were prepared from HEK293 cells transiently transfected with FLAG-tagged receptor constructs or pcDNA3 as control. The cells were manually harvested with a cell scraper in ice-cold PBS and homogenized using a Dounce. The homogenate was centrifuged at 500 rpm for 3 min at 4 °C. Subsequently, the supernatants were collected and centrifuged at 20,000 rpm at 4 °C for 30 min. The resulting membrane pellets were resuspended in 20 mM HEPES buffer containing 2 mM MgCl₂ and Complete protease inhibitor mixture (Roche Applied Science) and kept at -80 °C until used in [³⁵S]GTP γ S binding experiments or competition binding. The protein concentrations in each preparation were determined using the BCA protein assay kit (Pierce).

[³⁵S]GTP γ S Binding Assay—[³⁵S]GTP γ S binding experiments were carried out in white 96-well plates (Nunc) using the SPA-based method. A volume of membrane preparation (corresponding to 20 μ g of protein/well) was diluted in assay buffer (50 mM HEPES, 3 mM MgCl₂, 100 mM NaCl, 1 mM EGTA, 3 μ M

³ We used both numbering systems of Baldwin-Schwartz and Ballesteros (in this order and separated by a slash) when referring to positions within the helical domains.

Elucidation of $7\alpha,25$ -Dihydroxycholesterol Binding to EBI2

GDP, 10 $\mu\text{g/ml}$ saponin, and Complete inhibitor mix, pH 7.4). [^{35}S]GTP γS (1250 Ci/mmol, 12.5 mCi/ml) diluted in assay buffer was added to a final concentration of 1 nM and incubated 1 h at 30 °C. Subsequently, WGA PVT SPA beads (PerkinElmer Life Sciences) were added (final concentration of 2.8 mg/ml) followed by 30 min of incubation at room temperature on a plate shaker. Finally, the plates were centrifuged at 1500 rpm for 5 min, and the amount of radioactivity was determined using a Top Count scintillation counter (PerkinElmer Life Sciences). The level of unspecific binding was determined by adding unlabeled GTP γS at a final concentration of 40 μM . All experiments were carried out at least three times and in triplicate.

^3H 7 $\alpha,25$ -OHC Competition Binding Assay—[^3H]7 $\alpha,25$ -OHC competition binding experiments were carried out in white 96-half-well plates (Costar). 10 μl of WGA PVT SPA beads diluted in binding buffer (50 mM Tris-HCl, 5 mM MgCl₂, 100 mM NaCl, and 0.1% cyclodextrin, pH 7.4) to 20 mg/ml was added to each well. Subsequently, 30 μl of membrane preparation diluted in binding buffer to 0.67 mg/ml was added. After a 20-min incubation on a shaker at room temperature, 2.5 μl of ligand at 20 \times final concentration was added followed by addition of [^3H]7 $\alpha,25$ -OHC to a final concentration of 10 nM. The plates were sealed and, after 15 min on shaker, incubated at room temperature overnight. The following day, the plates were spun down at 1500 rpm for 5 min and counted in a TopCounter (PerkinElmer Life Sciences).

β -Arrestin Recruitment—Recruitment of β -arrestin was measured using the PathHunter β -arrestin assay (DiscoverRx). cDNA encoding M1-EBI2 WT was fused to the PK1 tag and the small fragment of β -galactosidase and cloned into pcDNA3.1+. Mutations were generated using the QuikChange protocol. Assays were performed in a CHO K1.A2-arrestin cell line stably expressing β -arrestin2 coupled to the β -gal large fragment. Cells were seeded out at 20,000 cells/well in 96-well plates and transfected the following day with 50 ng of DNA using FuGENE 6 reagent (0.15 μl /well). 48 h after transfection, cells were stimulated with varying concentrations of 7 $\alpha,25$ -OHC for 90 min. β -Arrestin recruitment was detected as β -gal activity 60 min after addition of chemiluminescent substrate.

Calcium Mobilization Assay—CHO-K1 cells stably transfected with G_{qi5} were seeded in black/clear bottom, poly-D-lysine-coated 384-well plates at a cell density of 10,000 cells/25 μl /well using culture medium. Cells were cultured for overnight at 37 °C and 5% CO₂. Culture medium was removed, and for cell loading, 20 μl per well of loading buffer (Calcium-5 no wash dye, Molecular Devices) were distributed into the wells, and the plates were incubated for 60 min at 37 °C in 5% CO₂. Compound dilutions were prepared in 90% DMSO, 10% water and finally transferred to assay buffer containing 0.1% cyclodextrin. Ten microliters of the compound was added to the cells, and the subsequent fluorescent changes were monitored for 3 min. Fluorescence was detected using a FDSS7000 (Hamamatsu). Two values of fluorescence calcium responses were exported as follows: F_{max} , the fluorescence at the peak, and F_{basal} , corresponding to the value prior to compound injection. From these two values, the calcium response is normalized with

respect to the calcium base-line values using $dF/F = (F_{\text{max}} - F_{\text{basal}})/F_{\text{basal}}$. The maximum dF/F is called E_{max} .

CREB Trans-reporter Luciferase Assay—HEK293 cells were seeded at 35,000 cells/well in 96-well plates and transiently transfected the following day with FLAG-tagged receptor constructs or pcDNA at the indicated concentrations along with the trans-activator plasmid pFA2-CREB, the reporter plasmid pFRluc, and in some experiments the chimeric G-protein G_{qi4}myr at 6, 30, and 50 ng/well, respectively. The latter is a promiscuous G protein that binds to G α_i -coupled receptors but activates the G α_q pathway. The CREB activity was determined 48 h after transfection using the SteadyLite substrate (PerkinElmer Life Sciences). Briefly, the cells were washed twice in Dulbecco's PBS (0.9 mM CaCl₂, 2.7 mM KCl, 1.5 mM KH₂PO₄, 0.5 mM MgCl₂, 137 mM NaCl, and 8.1 mM Na₂HPO₄), and the luminescence was measured 10 min after addition of the substrate using a TopCounter (PerkinElmer Life Sciences). All receptor constructs were tested at least three times in quadruples.

Enzyme-linked Immunosorbent Assay (ELISA)—HEK293 cells were transiently transfected with the indicated FLAG-tagged receptor constructs as described above. Forty eight hours after transfection, the cells were fixed in 4% formaldehyde for 10 min, washed three times in TBS, and blocked for 30 min with TBS containing 2% BSA. Subsequently, the cells were incubated with mouse anti-FLAG M1 antibody at 2 $\mu\text{g/ml}$ for 2 h in TBS supplemented with 1% BSA and 1 mM CaCl₂. After three washes in TBS containing 1% BSA and 1 mM CaCl₂, the cells were incubated for 1 h with goat anti-mouse horseradish peroxidase-conjugated antibody diluted 1:1000 in the same buffer as the primary antibody. Following washing, the immune reactivity was determined by addition of 3,3',5,5'-tetramethylbenzidine according to the manufacturer's instruction. All steps were carried out at room temperature, and all constructs were tested at least three times in quadruples.

EBI2 Homology Model—The sequence of the human EBI2 receptor was obtained from Uniprot (accession code p32249). The closest three-dimensional structure homologue of EBI2 with known structure, CXCR4 (Protein Data Bank code 3ODU) (21), was used as template structure. The TL4-lysozyme domain was deleted from the CXCR4 crystal structure, and the sequence alignment between EBI2 and the template was constructed using the bioinfo tools in the ICM software package (Molsoft LLC, La Jolla, CA). Because the quality of comparative homology models is highly dependent on the quality of the sequence alignment between the target and the template structure, manual inspections and minor adjustments were performed to ensure proper alignment of conserved class A G-protein-coupled receptor motifs, conserved generic fingerprints, and to avoid accidental gaps in the transmembrane region. Specifically, the obligatory disulfide bridge between the highly conserved CysIII:01/3.25 (Cys-104 in EBI2) in the extracellular part of TMIII and a Cys in extracellular loop 2 (Cys-181 in EBI2) formed in most 7TM receptors was manually aligned to the CXCR4 template to ensure that the disulfide bridge would be formed in the initial EBI2 homology model (see supplemental Fig. 1). During EBI2 model generation, all amino acid were subjected to a full side chain optimization to optimize their packing. Loop regions of the EBI2 model that were constructed

without a template were selected as the best scored loop structures assigned conformations from similar “fragments” in the ICM database of experimental structures.

In general, comparative homology models are considered to be associated with atomic position errors that impede the use of homology models for purposes that require atomic resolution data, such as drug design and protein-ligand interaction predictions. Thus, the initial EBI2 model was subjected to full-atom structure relaxation using the ROSETTA membrane force field (22) in Rosetta 3.2.1 (23) to capture the intrinsic flexibility of the receptor. A total of 1000 EBI2 models was generated, and from these the best 10 scoring models were selected as the receptor ensemble during the subsequent docking of 7 α ,25-OHC. Likewise, a ligand ensemble, including 20 conformations, was prepared in ICM within 3 kcal/mol of the global energy minimum using the MMFF force field and generalized born solvent as an implicit solvation model.

Docking of 7 α ,25-OHC—A full flexible docking of 7 α ,25-OHC to the EBI2 receptor was performed using ROSETTALIGAND (24) and the XML docking protocol described previously (25). Briefly, the protocol randomly selects a structure from the protein and the ligand ensemble, uniformly places and rotates the ligand within a defined docking sphere, and performs a simultaneous optimization of the ligand and the receptor using a Metropolis Monte Carlo simulated annealing algorithm. The center of the dockings sphere, which defines the “center” of the binding pocket, was placed between Arg-87, Tyr-116, and Tyr-260 which, based on mutational mapping, are suggested to be involved in ligand binding. The radius of the docking sphere, which defines the “size” of the pocket and the space within the center of the ligand, that can be placed and effectively sampled was set to 5 Å. A total of ~32,000 docking trajectories was generated.

Inaccuracies in the structural models due to incorrect backbone and side chain conformations, lack of explicit water molecules, approximations in the Rosetta force field, and sampling limitations in combination with an expected relatively small energy gap between the correct and incorrect docking poses preclude the use of ligand-protein interaction energies for accurate determination of the global minima. Realizing this, the ensemble of ligand receptor complexes was initially filtered based on distance constraints derived from the biochemical binding data. The data (see under “Results”) suggest that Tyr-116 and Tyr-260 likely are involved in hydrogen bond interactions with at least one of the three hydroxyl groups in the ligand. Thus, receptor ligand complexes in which any of the three ligand hydroxyl oxygen atoms were within 5 Å of the oxygen atoms in the tyrosine side chains were accepted. As Phe-111 is not important for 7 α ,25-OHC function (see under “Results”), docking poses in which the distance between C $^{\epsilon}$ of Phe-111 and any ligand heavy atom less than 5 Å were discarded. Among the ~32,000 ligand receptor complexes, 216 passed the filter criteria proposed by the experimental mutational data.

The resulting filtered structures were aligned with the CE algorithm (26) as implemented by PyMOL (The PyMOL Molecular Graphics System, version 1.5.0.1 Schrödinger, LLC). The ligand-ligand heavy atom root mean square distance matrix was computed using our own scripts, and the ligand

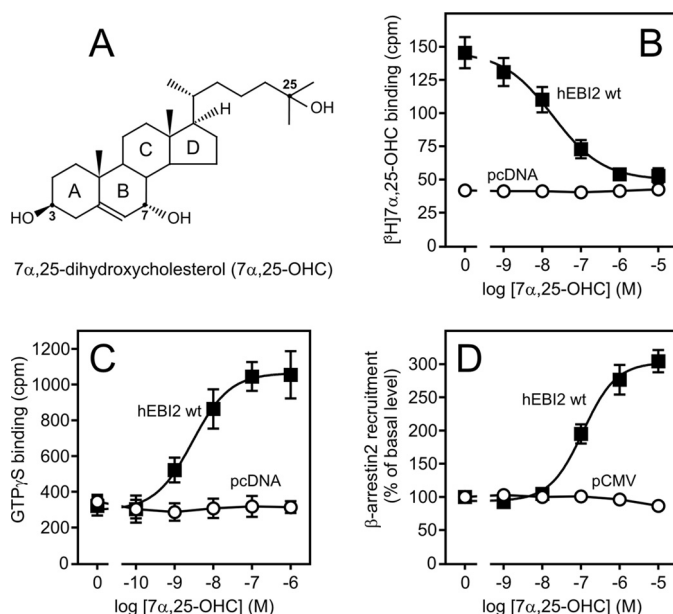


FIGURE 1. 7 α ,25-OHC activates EBI2 with high potency. *A*, two-dimensional projection of the high potency EBI2 agonist 7 α ,25-OHC. The three hydroxyl groups at position 3 (in β -conformation), 7 (in α -conformation), and 25 are labeled as well as the rings of the steroid backbone (numbered A–D). *B*, [3 H]7 α ,25-OHC homologous competition binding assay. Binding was measured using WGA-coupled SPA beads and membranes from HEK293 cells transiently transfected with FLAG-tagged human EBI2 (hEBI2; solid squares) or pcDNA3 (open circles) as control. Results represent means \pm S.E. of raw data from four independent experiments. The final assay concentration of [3 H]7 α ,25-OHC was 10 nM. *C*, 7 α ,25-OHC induced [35 S]GTP γ S binding to membranes isolated from CHO FLP-IN cells stably transfected with hEBI2 (solid squares) or pcDNA5 (open circles). Results represent means \pm S.E. of raw data from four independent experiments. *D*, 7 α ,25-OHC-induced β -arrestin2 recruitment in β -arrestin- β -galactosidase-expressing CHO cells transiently transfected with hEBI2 (solid squares) or pCMV (open circles). The data are normalized to basal recruitment levels (*i.e.* in absence of 7 α ,25-OHC) and are presented in percent as means \pm S.E. from four independent experiments.

binding poses were clustered using a hierarchical agglomerative clustering algorithm implemented in BCL::Cluster (27) using a clustering threshold of 3.0 Å, which identified a total of 60 clusters.

RESULTS

7 α ,25-OHC Binding, Importance of Arg-87 at Position II:20/2.60—For structure-function analysis, we focused on the most potent EBI2-activating oxysterol, 7 α ,25-OHC (12, 13). This molecule carries hydroxyl groups at position 3 in the A-ring (β conformation), position 7 (α conformation) in the B-ring, and at position 25 in the *iso*-octyl side chain (Fig. 1A). As reported previously (12, 13), the radioligand [3 H]7 α ,25-OHC bound selectively to membranes isolated from HEK293 cells transiently expressing human EBI2 (hEBI2) but not to pcDNA-transfected counterparts. Radioligand binding was displaced by 7 α ,25-OHC with an IC $_{50}$ value of 24 ± 1.6 nM (Fig. 1B). Similar results were observed with membranes from CHO cells stably expressing hEBI2 (data not shown). In GTP γ S binding assays, 7 α ,25-OHC induced G protein activation with an EC $_{50}$ value of 1.0 ± 0.1 nM in hEBI2-containing membranes but not in pcDNA controls (Fig. 1C). Furthermore, activation of hEBI2 by 7 α ,25-OHC resulted in a dose-dependent recruitment of β -arrestin (Fig. 1D) and Ca $^{2+}$ mobilization (Table 1) with EC $_{50}$ values of 83 ± 1.3 and 16 ± 2.7 nM, respectively. In all

Elucidation of 7 α ,25-Dihydroxycholesterol Binding to EBI2

TABLE 1

Receptor expression together with potencies and affinities of 7 α ,25-OHC on a selection of EBI2 mutations

From left: residue mutated and the position in the receptor, surface expression, and potencies of 7 α ,25-OHC (depicted as $-\log(\text{EC}_{50})$) in three different functional assays (β -arrestin recruitment, GTP γ S, and Ca²⁺ mobilization) and the affinity of 7 α ,25-OHC (depicted as $-\log(\text{IC}_{50})$). The data are presented as mean \pm S.E.M., and the number of independent experiments is indicated (*n*). Cell surface expression as measured by ELISA is presented as mean \pm S.E.M. of raw data where background (pcDNA-transfected cells) has been subtracted. The -fold change in surface expression compared to hEBI2 WT is shown (Δ abs). ND, not determined; N/A, not applicable (no curve or binding).

	Resid.	Position	Mutation	Surface exp. abs \pm S.E.M.	Δ abs. (n)	β -arrestin $-\log\text{EC}_{50} \pm \text{SEM}$ (n)	GTP γ S $-\log\text{EC}_{50} \pm \text{SEM}$ (n)	Ca ²⁺ mob. $-\log\text{EC}_{50} \pm \text{SEM}$ (n)	Binding $-\log\text{IC}_{50} \pm \text{SEM}$ (n)
		EBI2 wt		0,14 \pm 0,01	1,0 (7)	7,1 \pm 0,1 (9)	9,0 \pm 0,1 (4)	7,8 \pm 0,1 (4)	7,6 \pm 0,2 (12)
TM-II	D77	II:10 / 2,50	D77A	0,14 \pm 0,02	1,0 (4)	<5 (4)	ND	ND	7,6 \pm 0,1 (3)
			D77R	0,10 \pm 0,01	0,7 (4)	7,7 \pm 0,4 (5)	ND	ND	7,4 \pm 0,1 (3)
	R87	II:20 / 2,60	R87A	0,12 \pm 0,01	0,9 (3)	<5 (3)	5,3 \pm 0,2 (3)	ND	N/A (3)
			R87K	0,08 \pm 0,01	0,5 (3)	6,6 \pm 0,4 (3)	7,4 \pm 0,3 (3)	ND	8,1 \pm 0,5 (3)
TM-III	Y90	II:23 / 2,63	Y90A	0,07 \pm 0,00	0,5 (6)	6,1 \pm 0,3 (4)	ND	ND	ND
			F111	0,11 \pm 0,01	0,7 (3)	6,8 \pm 0,2 (3)	9,0 \pm 0,2 (4)	ND	ND
	F111	III:08 / 3,32	F111A	0,07 \pm 0,01	0,5 (3)	6,8 \pm 0,1 (3)	ND	ND	ND
			F111Y	0,17 \pm 0,02	1,2 (6)	<5 (4)	5,8 \pm 0,1 (4)	<5 (4)	8,1 \pm 0,5 (3)
	Y112	III:09 / 3,33	Y112A	0,14 \pm 0,01	1,0 (6)	6,8 \pm 0,2 (4)	8,5 \pm 0,2 (4)	7,6 \pm 0,1 (4)	7,7 \pm 0,2 (3)
			T115	0,11 \pm 0,01	0,8 (4)	5,9 \pm 0,5 (2)	ND	7,6 \pm 0,1 (4)	ND
	T115	III:12 / 3,36	T115A	0,09 \pm 0,01	0,6 (4)	6,4 \pm 0,1 (3)	ND	ND	ND
			T115F	0,13 \pm 0,01	0,9 (6)	<5 (4)	<5 (4)	5,3 \pm 0,1 (4)	N/A (3)
Y116	III:13 / 3,37	Y116A	0,16 \pm 0,02	1,1 (5)	<5 (4)	<5 (4)	<5 (4)	N/A (3)	
		Y116F	0,12 \pm 0,02	0,9 (4)	6,5 \pm 0,2 (3)	ND	6,9 \pm 0,1 (4)	ND	
TM-V	Y205	V:13 / 5,47	Y205A	0,09 \pm 0,01	0,6 (4)	7,0 \pm 0,2 (3)	ND	7,8 \pm 0,1 (4)	ND
			Y205F	0,10 \pm 0,02	0,7 (4)	<5 (4)	<5 (4)	<5 (4)	N/A (3)
TM-VI	Y260	VI:16 / 6,51	Y260A	0,16 \pm 0,02	1,1 (4)	<5 (4)	5,6 \pm 0,2 (4)	<5 (4)	N/A (3)
			Y260F	0,10 \pm 0,01	0,7 (4)	6,7 \pm 0,2 (4)	ND	ND	ND
TM-VII	Q287	VII:02 / 7,32	Q287A	0,15 \pm 0,02	1,0 (4)	6,1 \pm 0,7 (3)	ND	ND	ND
			H291	0,15 \pm 0,02	1,0 (4)	6,1 \pm 0,7 (3)	ND	ND	ND
Poly	D77-	II:10- / 2,50-	D77A-	0,06 \pm 0,01	0,4 (4)	<5 (4)	ND	ND	N/A (3)
			R87	0,16 \pm 0,01	1,2 (4)	7,6 \pm 2,5 (5)	ND	ND	7,0 \pm 0,2 (3)
		II:10- / 2,50-	D77R-						
		II:20 2,60	R87A						
		II:20 2,60	R87A						

four assays, the half-maximal concentration values were in close agreement with previous reports (12, 13).

For the mutational screening, we focused on residues facing the main binding pocket (Fig. 2 and Table 1). This included residues at positions known to be important for ligand binding in other 7TM receptors as well as residues capable of hydrogen bonding. As GTP γ S binding was only detectable in membranes from stably transfected CHO cells, we used β -arrestin recruitment as a functional readout for the mutational screening. Binding experiments and generation of stably transfected CHO cell clones for GTP γ S binding were subsequently performed for hits. In addition, Ca²⁺ mobilization was measured for most hits. The cell surface expression of all constructs was determined by ELISA against their N-terminal M1 FLAG tag (Table 1).

We initially focused on the Arg at position II:20/2.60 (residue number R87) as we have previously shown that this residue is important for EBI2 activity (19). This residue is located in the top of TM-II near the interface between the helix and the extracellular environment. Furthermore, the recent crystal structures of CXCR4 (21) and the S1P1 receptor (28) revealed that the II:20/2.60 side chain protrudes into the binding pocket (see below) and not toward the membrane bilayer as anticipated previously. Interestingly, when Arg-87 was mutated to an Ala, the 7 α ,25-OHC-induced β -arrestin recruitment was virtually abolished (Fig. 3A). This was also observed at the level of G protein activation with a decrease in the GTP γ S EC₅₀ value of \sim 5000-fold (Fig. 3B). Competition binding experiments

revealed that this was a result of attenuated binding as no radioligand binding was detectable in EBI2 R87A membranes as opposed to EBI2 WT membranes (Fig. 3C). The lack of binding was not a result of low or abolished cell surface expression as the expression level of the mutant was WT-like (Table 1). As opposed to the R87A mutation, substituting Arg-87 with a Lys only slightly affected EBI2 activation (Fig. 3, A–C) indicating that the charge and/or the hydrogen bonding properties of Arg-87 is important for agonist binding.

7 α ,25-OHC Interacts with Tyr-112 and Tyr-116 in TM-III and Tyr-260 in TM-VI—Based on the distances between the OH groups in 7 α ,25-OHC, we selected a group of residues in TM-III, -VI, and -VII in the vicinity of Arg-87. In TM-III, two Tyr residues are found one helix turn apart at positions III:09/3.33 (Tyr-112) and III:13/3.37 (Tyr-116) (Fig. 2A). To test whether these are involved in 7 α ,25-OHC binding, we introduced Ala or Phe substitutions at both positions. For Tyr-112, Ala substitution had a profound effect on β -arrestin recruitment (Fig. 3D), G protein activation (Fig. 3E), binding (Fig. 3F), and Ca²⁺ mobilization (Table 1), although the mutant was expressed well (Table 1). On the contrary, no change was observed upon Phe substitution (Fig. 3, D–F, and Table 1) indicating that Tyr-112 contributes to 7 α ,25-OHC binding through aromatic or other hydrophobic interactions. Interestingly, the neighboring Phe-111 at position III:08/3.32 was not important for agonist-induced activation (Table 1) despite being crucial for the activity of the EBI2 inverse agonist/antagonist GSK682753A (29). For Tyr-116 at position III:13/3.37, β -arres-

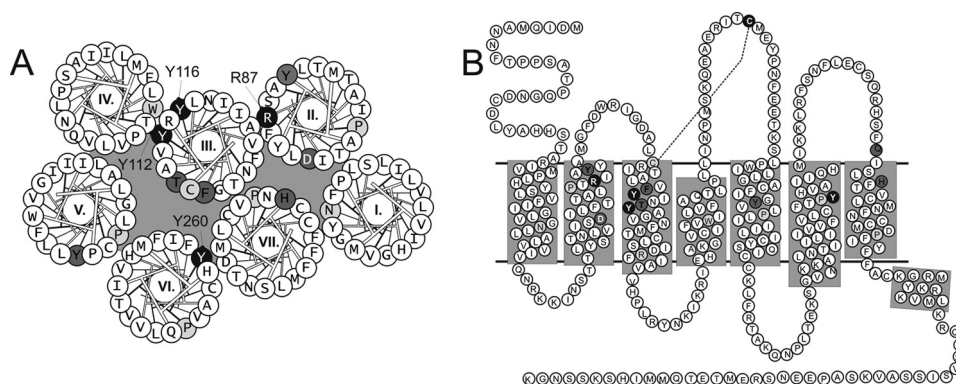


FIGURE 2. **Helical wheel (A) and snake-diagram (B) of the human EBI2.** Mutated residues are indicated in *dark gray* (no effect on 7 α ,25-OHC binding) or *black with white letters* (agonist anchor points Arg-87, Tyr-112, Tyr-116, and Tyr-260). The conserved 7TM receptor family residues in each helix are colored in *light gray* with the exception of Asp-77 (position II:10/2.50 in TM-II), which is *dark gray with white lettering* as this was included in the mutational analysis. Note that the orientation of the anchor residues is depicted schematically only (compare with Fig. 4).

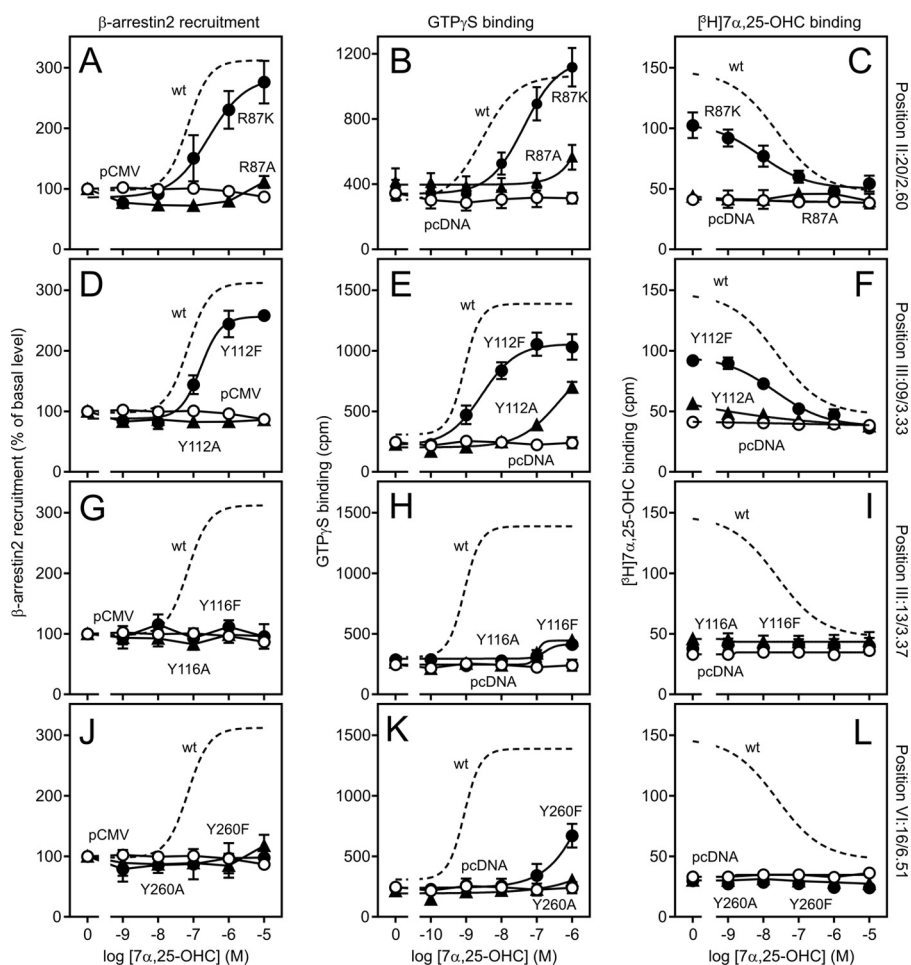


FIGURE 3. **Arg-87, Tyr-112, Tyr-116, and Tyr-260 are highly important for 7 α ,25-OHC binding.** 7 α ,25-OHC-induced β -arrestin2 recruitment (*left column*), GTP- γ S binding (*middle column*), and displacement of [3 H]7 α ,25-OHC binding (*right column*) for the FLAG-tagged hEBI2 mutants R87A/R87K at position II:20/2.60 (A–C), Y112A/Y112F at position III:09/3.33 (D–F), Y116A/Y116F at position III:13/3.37 (G–I), and Y260A/Y260F at position VI:16/6.51 (J–L). EBI2 WT curves are indicated as a *dashed line*, Ala substitution as *solid triangles*, Phe/Lys substitutions as *solid circles*, and controls as *open circles*. The data are presented as described in Fig. 1 and are at least from three independent experiments.

tin recruitment (Fig. 3G), G protein activation (Fig. 3H), and Ca²⁺ mobilization (Table 1) were abolished both upon Ala or Phe substitution. This was a result of a lack of binding (Fig. 3I) rather than attenuated cell surface expression as both constructs were expressed at WT levels (Table 1) indicating that Tyr-116 possibly interacts with 7 α ,25-OHC through hydrogen

bonding with an OH group. Finally, using distance constraints, we identified a set of residues in TM-VI and -VII that could potentially constitute the third OH group anchor point. Whereas the selected TM-VII residues did not seem to be important for agonist function (Table 1), both β -arrestin recruitment (Fig. 3J), G protein activation (Fig. 3K), and Ca²⁺

Elucidation of $7\alpha,25$ -Dihydroxycholesterol Binding to EBI2

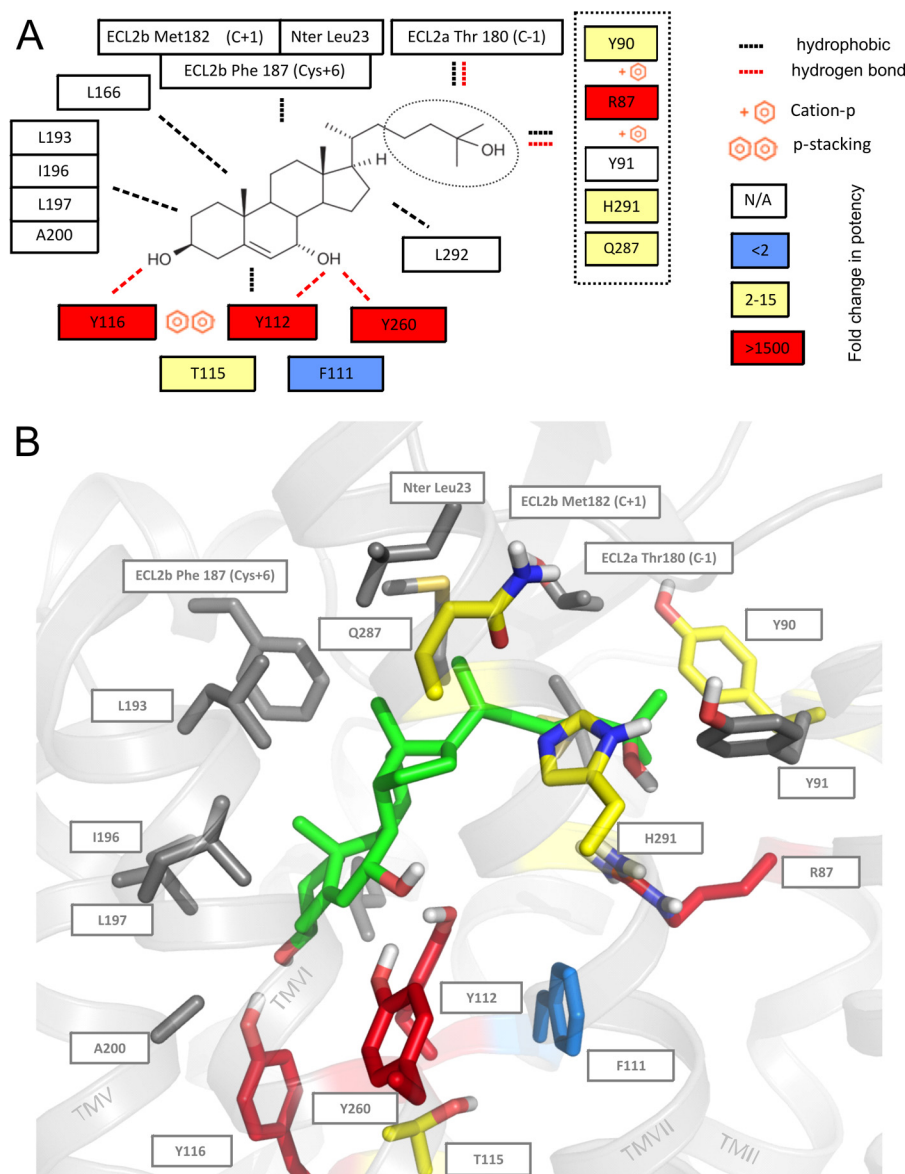


FIGURE 4. **Proposed binding mode of $7\alpha,25$ -OHC in EBI2.** *A*, two-dimensional ligand plot summarizing the interactions found in the largest cluster obtained by filtering 32,000 docking trajectories according to selected mutational data. Multiple contact opportunities are shown where several mutually exclusive contacts are possible. Cation- π , π -stacking interactions, hydrophobic contacts (black dashed lines), and hydrogen bonds (red dashes) are shown and the fold change in potency upon Ala substitution is indicated for some residues. The ring system is situated between TM-III and -VII. Contacts to this part of the molecule is conserved with the exception of Tyr-112 (position III:09/3.33), which based on mutational mapping most likely forms hydrophobic contacts to the agonist or stabilizes Tyr-116 (III:13/3.37) through π -stacking interactions. The aliphatic chain carries most of the flexibility in the cluster and can contact a range of residues through both hydrogen bonds and hydrophobic interactions. *B*, representative binding mode of a ligand in the largest cluster.

mobilization (Table 1) were profoundly affected when the Tyr at position VI:16/6.51 (Tyr-260) was substituted with either Ala or Phe. As described previously, this was a result of abolished binding (Fig. 3L) and not the lack of cell surface expression (Table 1). Thus, as with Tyr-116, Tyr-260 likely interacts with $7\alpha,25$ -OHC through hydrogen bonding to an OH group.

Binding Mode of $7\alpha,25$ -OHC—To test the binding mode further, we conducted a docking simulation of $7\alpha,25$ -OHC binding to EBI2 using ROSETTALIGAND and carefully analyzed the five largest clusters (designated cluster 1–5) containing 42, 21, 13, 9, and 9 agonist-receptor complexes, respectively. The average ligand-protein interface energy in cluster 4 was significantly higher than that of clusters 1 and 2. The best scoring conformations was found in the largest cluster, and these

ranked within the top 0.5% of the unfiltered ensemble. In all analyzed clusters, the cholesterol ring system of the ligand was located in a predominantly hydrophobic aromatic pocket between the transmembrane helices TM-III and -VII.

Interestingly, in the largest cluster, the 3β -OH group of $7\alpha,25$ -OHC forms hydrogen bonds with the hydroxyl group of the Tyr-116 (position III:13/3.37) side chain (Fig. 4). Moreover, the 7α -OH group is involved in hydrogen bond formation with the hydroxyl group of the Tyr-260 (position VI:16/6.51) side chain. This binding mode is in agreement with the mutational analysis (Fig. 3 and Table 1). Furthermore, it is also consistent with pharmacological data from the initial deorphanization studies (12, 13) in which a 40-fold decrease in binding affinity was observed comparing $7\alpha,25$ -OHC and $7\beta,25$ -OHC.

However, inconsistencies with the mutational data were also observed. Thus, in a number of cases the OH group of the Tyr-112 (position III:09/3.33) side chain forms hydrogen bonds with the 7 α -OH group which is not in agreement with the mutational data as the Y112F mutation did not affect binding and function (Fig. 3). Instead, the importance of the aromatic part of position III:09/3.33 can either be explained by the formation of stabilizing π -stacking interactions to Tyr-116 or hydrophobic interactions with the agonist as observed in other clusters.

Although the cholesterol scaffold adopts a well defined pose, the distal 25-OH group in the flexible aliphatic chain shows several possible hydrogen bond interactions within the complex. In some cases the 25-OH group forms hydrogen bond contacts to backbone atoms of ECL2 or the Thr-180 side chain in ECL2. In these cases, C26 and C27 atoms often form hydrophobic interactions with Tyr-90 (at position II:23/2.63) and Tyr-91 (II:24/2.64), which are located one helical turn above Arg-87. In other cases, the 25-OH group is flipped over and forms hydrogen bond interactions to either of the OH groups in Tyr-90 and Tyr-91 (Fig. 4) or to His-291 (position VII:03/7.36) and Gln-287 (position VII:02/7.32) located just opposite Tyr-91. Ala substitution of Tyr-90, His-291, or Gln-287 resulted in an \sim 10-fold reduction in potency (Table 1) indicating that these residues could contribute to ligand binding. In a few cases, the 25-OH group made direct hydrogen bond contact to Arg-87. However, only suboptimal hydrogen bond geometries between the 25-OH group and the guanidine side chain were observed suggesting that the importance of Arg-87 could be indirect. Thus, Arg-87 could *e.g.* bind 7 α ,25-OHC via an intermediate water molecule (not present in the model). Indeed, the increasing number of 7TM receptor crystal structures indicates that water plays an essential role in the functionally important hydrogen bond network between a ligand and receptor residues within the binding pocket. Alternatively, Arg-87 could be involved in stabilization of adjacent residues directly involved in ligand binding or lock the receptor in a more active conformation thereby promoting agonist binding. In clusters 2–5, some of the same interactions were observed in some cases but did in general not agree as well with the mutational data as cluster 1. In conclusion, our docking simulation suggests that the 3 β -OH group interacts with Tyr-116, 7 α -OH with Tyr-260, and 25-OH with Arg-87 (either directly or indirectly), Tyr-90, Tyr-91, Gln-287, and/or His-291.

Importance of Position II:10/2.50 for EBI2 Activation, Reintroduction of 7 α ,25-OHC Binding—A highly conserved Asp is found at position II:10/2.50 in the rhodopsin-like subfamily of 7TM receptors (Fig. 2). To investigate the importance of this residue (Asp-77 in EBI2) for receptor activation, we mutated it to Ala or Arg. As seen in Fig. 5A, the D77A substitution completely abolished 7 α ,25-OHC-induced β -arrestin recruitment. This was not the result of attenuated binding, however, as the radioligand still bound to membranes expressing the mutant and was displaced with an IC₅₀ value equivalent to WT (Fig. 5B and Table 1). Similarly, the D77R mutant also bound the radioligand with WT-like affinity. However, contrary to D77A, it still recruited β -arrestin and even with a slight increase in potency (4-fold; Fig. 5A). This indicates that Asp-77 is not important for 7 α ,25-OHC binding but rather is essential for the activation

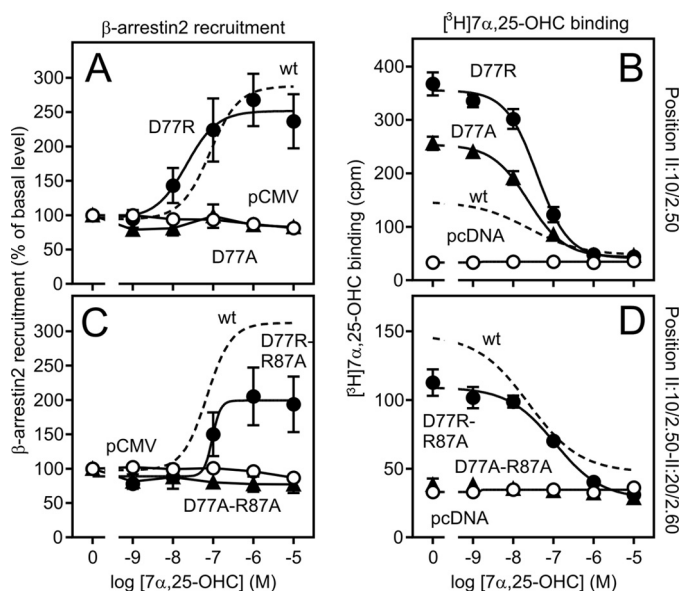


FIGURE 5. Importance of Asp-77 (position II:10/2.50) for receptor activation and reintroduction of 7 α ,25-OHC binding. A, 7 α ,25-OHC-induced β -arrestin2 recruitment for the FLAG-tagged hEBI2 mutants D77A (solid triangles) and D77R (solid circles). The EBI2 WT curve and the control are indicated as a dashed line and with open circles, respectively. The data are normalized to basal recruitment level (*i.e.* in absence of 7 α ,25-OHC) and are presented in percent as means \pm S.E. from at least four independent experiments. B, [³H]7 α ,25-OHC homologous competition binding for the mutants in A. Results represent means \pm S.E. of raw data from at least four independent experiments. C, 7 α ,25-OHC-induced β -arrestin2 recruitment for the FLAG-tagged hEBI2 double mutants D77A/R87A (solid triangles) and D77R/R87A (solid circles). The data are normalized to basal recruitment level (*i.e.* in absence of 7 α ,25-OHC) and are presented in percent as means \pm S.E. from at least four independent experiments. D, [³H]7 α ,25-OHC homologous competition binding for the mutants in C. Results represent means \pm S.E. of raw data from at least four independent experiments.

mechanism of EBI2 by hydrogen bonding to one or more residues. Given the importance of Arg-87 (position II:20/2.60) for 7 α ,25-OHC binding and Asp-77 (II:10/2.50) for the activation mechanism, we examined their significance in combination. Thus, we generated two double mutants, D77A/R87A and D77R/R87A, and measured β -arrestin recruitment and radioligand binding. Interestingly, whereas the D77A/R87A mutant was not able to recruit β -arrestin or bind 7 α ,25-OHC, the D77R/R87A mutant bound the agonist and was also able to recruit β -arrestin with a half-maximal concentration close to WT (Fig. 5, C and D). Thus, introducing an Arg at position II:10/2.50 in the EBI2 R87A mutant (which does not bind the agonist, Fig. 3A) reconstitutes agonist binding. Although this likely is an indirect effect given the distance between II:10/2.50 and the other anchor residues, it emphasizes the important role of TM-II in both agonist binding and activation of EBI2.

Position II:20/2.60 as Possible Anchor Point in Other 7TM Receptors—Besides the conserved Asp at position II:10/2.50, a Pro residue is found at the top of TM-II in 78% of rhodopsin-like 7TM receptors. However, this is found at one of two adjacent positions, namely II:18/2.58 (41% conserved) or II:19/2.59 (37%) (30). Importantly, these two positions are always aligned in the receptor structures due to an insertion at position II:16 in ProII:19 receptors resulting in a bulge on TM-II as evident from the 7TM receptor crystal structures. Accordingly, position II:20 is oriented toward the lipid bilayer in ProII:19 receptors, exem-

Elucidation of 7 α ,25-Dihydroxycholesterol Binding to EBI2

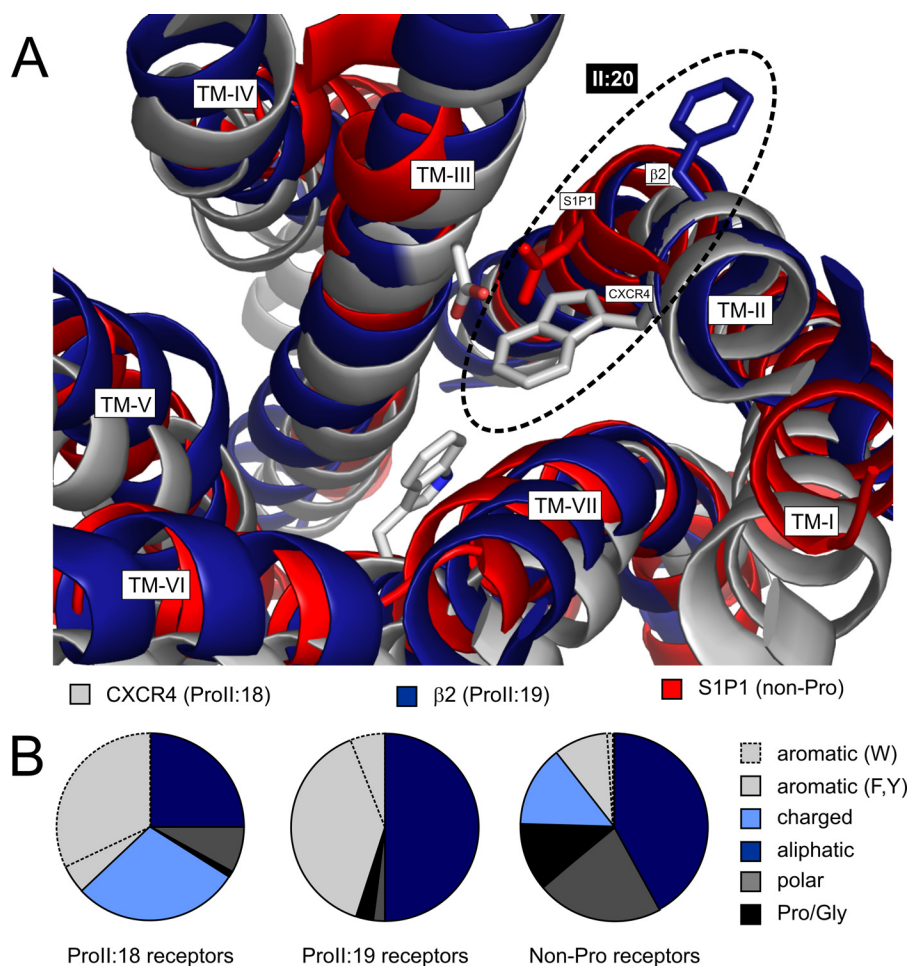


FIGURE 6. Position and orientation of residue II:20/2.60. *A*, view from the extracellular side of the human CXCR4 (gray; Protein Data Bank code 3ODU), the human β_2 -adrenoreceptor (dark blue; Protein Data Bank code 2RH1), and the human S1P1 receptor (red; Protein Data Bank code 3V2Y) crystal structures as aligned by PyMOL software. All loops as well as helix 8 have been omitted for clarity. Residue II:20/2.60 in TM-II (a Trp in CXCR4, a Phe in the β_2 -adrenoreceptor, and an Asn in the S1P1 receptor) is indicated at the top (dashed ellipse). In CXCR4 and the S1P1 receptor, the II:20/2.60 side chain is twisted $\sim 60^\circ$ compared with the β_2 -adrenoreceptor and faces the binding pocket. This is caused by the presence of the TM-II Pro at position II:18/2.58 in CXCR4 and the absence of a TM-II Pro in the S1P1 receptor. For the β_2 -adrenoreceptor, the TM-II Pro is found at position II:19/2.59, and the side chain of II:20/2.60 consequently faces the lipid bilayer. For reference, the location of the functionally important Asp at position III:08/3.32 and the Trp at VI:13/6.48 of the β_2 -adrenoreceptor have been included (in gray) as well as the helix numbers. *B*, amino acid frequency in ProII:18 receptors (left), ProII:19 receptors (middle), and non-Pro receptors (right). The aromatic residues Phe and Tyr are indicated in light gray; Trp in light gray with dashed lines; charged residues (Asp, Glu, Arg, Lys, and His) in light blue; aliphatic (Ala, Leu, Iso, Val, and Met) in dark blue; polar (Asn, Gln, Cys, Ser, and Thr) in dark gray, and Pro or Gly in black.

plified by the β -adrenergic receptors (31, 32) but oriented toward the binding pocket in ProII:18 receptors as exemplified by CXCR4 (21). Furthermore, very recently, the first non-Pro receptor, the S1P1 receptor, was crystallized (28). Interestingly, the II:20/2.60 side chain is oriented the same way as in ProII:18 receptors (e.g. CXCR4) (Fig. 6A). Accordingly, the orientation of II:20/2.60 is also reflected in the amino acid distribution at this position in ProII:18, ProII:19, and non-Pro receptors (Fig. 6B). For instance, charged amino acids at II:20/2.60 are only found in ProII:18 and non-Pro receptors (90% of which are positively charged), and polar residues are furthermore much more frequent. On the contrary, aliphatic residues are more common at II:20/2.60 in ProII:19 receptors (Fig. 6B).

To examine whether the importance of II:20/2.60 for agonist binding also extended to other receptors, we searched the human 7TM receptor repertoire for receptors containing a positively charged residue at II:20/2.60. In total, we identified 29 receptors (Table 2). This group contained several 7TM recep-

tor subfamilies such as the free fatty acid receptors, the proteinase-activated receptors, and the cysteinyl leukotriene receptors (CysLTs), in addition to several orphan receptors. Two things are notable. First, the majority of these receptors are activated either by lipids (e.g. EBI2, FFAR1–3, and CysLT1–2) or nucleotides (e.g. P2Y12–14). Second, they are all ProII:18 receptors, and the II:20/2.60 side chain thus faces the binding pocket providing a putative anchor point. We initially chose to focus on the CysLT1 and -2 and mutated the Arg at II:20/2.60 (Arg-79 in CysLT1 and Arg-94 in CysLT2) to either Ala or Lys. Whereas the CysLT WT receptors were activated by LTD₄ with EC₅₀ values of 1.7 ± 0.9 and 2.1 ± 0.3 nM, respectively, no activation was observed for the Ala mutants (Fig. 7, A and C). The Lys mutants were activated, although with an ~ 400 -fold (CysLT1) and ~ 40 -fold (CysLT2) decrease in potency compared with the WT receptors. This was not due to expression failure as all the mutants were present at the cell surface, although the CysLT1 mutants were at lower levels than WT (insets Fig. 7, B and D). We subsequently performed homologous competition binding

TABLE 2**The 29 human 7TM receptors containing an Arg or a Lys at position II:20/2.60**

The receptor name, any commonly used aliases, type (Arg or Lys), and generic number of the residue at II:20/2.60, endogenous agonist(s), and G-protein coupling are presented. Ligand abbreviations: 2-AG, 2- arachidonoylglycerol; ANM, anandamide; fMLP, formyl-Met-Leu-Phe; FPP, farnesyl pyrophosphate; LCFA, long chain fatty acid; LPA, lysophosphatidic acid; LPI, lysophosphatidyl-L-inositol; lyso-PS, lysophosphatidyl-L-serine; NAG, N-arachidonoylglycine; S1P, sphingosine 1-phosphate; SCFA, short chain fatty acid. The parentheses around the GPR55 ligands denote discrepancy among published studies.

Receptor	Aliases	II:20/2.60	Agonists	Coupling
CysLT1	HG55	Arg-79	LTC4, LTD4, LTE4	G α_q
CysLT2	HG57	Arg-94	LTC4, LTD4, LTE4	G α_q
EBI2	GPR183	Arg-87	7 α ,25-OHC	G α_i
FFAR1	GPR40	Lys-62	LCFA	G α_q
FFAR2	GPR43	Lys-65	SCFA	G α_p , G α_q
FFAR3	GPR41	Arg-71	SCFA	G α_i
FPR3	FPRH1	Arg-81	fMLP	Unknown
GPR17		Arg-115	UDP-nucleotides	G α_i
GPR18		Arg-78	Orphan	Unknown
GPR20		Arg-109	Orphan	G α_i
GPR34		Arg-110	Lyso-PS	G α_i
GPR55		Lys-80	(2-AG, ANM, LPI)	G α_q , G $\alpha_{12/13}$
GPR81	FKSG80	Arg-71	L-Lactate	G α_i
GPR87	GPR95	Arg-97	LPA	G α_q
GPR171	H963	Lys-70	Orphan	Unknown
GPR174	FKSG79	Arg-75	Orphan	Unknown
LPA4	GPR23, P2Y9	Lys-95	LPA	G α_s , G α_q , G $\alpha_{12/13}$
LPA5	GPR92, GPR93	Arg-78	LPA, FPP, NAG	G α_s , G α_q , G $\alpha_{12/13}$
LPA6	P2Y5	Arg-73	LPA	G $\alpha_{12/13}$
MrgX4	SNSR6	Arg-73	Enkephalin	G α_q
OXER1	TG1019	Arg-148	Oxoecicosanoid	G α_i
P2Y10		Arg-90	LPA, S1P	Unknown
P2Y12	P2Y(ADP)	Lys-80	ADP	G α_i
P2Y13	GPR86, GPR94	Lys-99	ADP	G α_i
P2Y14	GPR105	Lys-77	UDP-sugars	G α_i
PAR1		Lys-158	Thrombin	G α_p , G α_q , G $\alpha_{12/13}$
PAR2		Lys-131	Trypsin	G α_p , G α_q , G $\alpha_{12/13}$
PAR3		Lys-149	Thrombin	G α_p , G α_q , G $\alpha_{12/13}$
PAR4		Arg-132	Thrombin	G α_p , G α_q , G $\alpha_{12/13}$

measuring the extent of LTD₄ binding. For the CysLT WT receptors, LTD₄ displaced [³H]LTD₄ with IC₅₀ values of 0.9 ± 0.5 nM (CysLT1) and 10 ± 1.7 nM (CysLT2) (Fig. 7, B and D). On the contrary, neither of the Ala mutants bound [³H]LTD₄ in agreement with the results from the functional assay. The Lys mutants did bind [³H]LTD₄ but to a limited degree in both cases (32 and 39% of CysLT1 and CysLT2 WT, respectively) and displayed IC₅₀ values of 74 ± 2.3 nM (CysLT1) and 166 ± 4.6 nM (CysLT2). In addition, we also performed these experiments with LTC₄ and obtained virtually the same results (data not shown). Finally, we tested the importance of II:20/2.60 for the nucleotide-activated P2Y12 and P2Y14, which contains a Lys at this position (Lys-80 and Lys-77, respectively). UDP-galactose activated P2Y14 WT and the Arg mutant with similar potencies (EC₅₀ values of 0.1 ± 0.02 and 0.08 ± 0.01 μM, respectively) (Fig. 7E). On the contrary, the agonist activated the Ala mutant with a 50-fold decrease in potency. Interestingly, this was also observed for P2Y12. Thus, whereas the Arg mutant was activated by ADP with WT-like potency, the Ala mutant exhibited a 100-fold decrease in potency (Fig. 7F). Although it is not feasible to do binding experiments due to the low potency of the P2Y agonists, these results demonstrate that the II:20/2.60 residue, as in EBI2 and the CysLTs, is highly important for activation of these receptors.

DISCUSSION

Here, we present the first molecular characterization of oxysterol binding to a 7TM receptor, namely the binding mode of 7 α ,25-OHC to EBI2. The mutational analysis identified receptor residues Arg-87 in TM-II (position II:20/2.60), Tyr-116 in TM-III (III:13/3.37), and Tyr-260 in TM-VI (position VI:16/

6.51) as being of particular importance for agonist binding to EBI2 (Fig. 3). In line with these results, the docking simulation of 7 α ,25-OHC binding suggests that the 3 β -OH group interacts with Tyr-116, the 7 α -OH group with Tyr-260, and the 25-OH group with Arg-87 (directly or indirectly), Tyr-90, Tyr-91, Gln-287, and/or His-291 (Fig. 4). Structure-activity relationship data from the EBI2 deorphanization studies showed that changing the conformation of the 7-OH group from α to β had a greater impact on the affinity than changing the position of 25-OH group from 25 to 27 (12, 13) thus suggesting that the former is relatively more important for agonist binding than the latter. Accordingly, the interaction between 7 α and Tyr-260 at position VI:16/6.51 seems to have the largest impact on agonist binding and receptor activation. This aligns well with the observation that the major helical movement during receptor activation occurs in TM-VI. Specifically, the lower part of this helix swings outward and thereby creates space for G protein binding as evident from both crystallographic (32, 33) and biophysical (34) data. Furthermore, position VI:16/6.51 has been shown to be crucial for the activity of several other 7TM receptors. For instance, the Phe at VI:16/6.51 in the ghrelin receptor is believed to be part of a functionally important aromatic cluster between residues on the inner face of TM-VI and -VII that constrains the receptor in an active conformation (35, 36). In addition, VI:16/6.51 constitutes one of the anchor points in activating metal ion-binding sites engineered into several receptors (37, 38). Interestingly, position VI:16/6.51 is also involved in ligand binding in the S1P1 receptor that, as EBI2, is activated by lipids. As evident from the recent crystal structure, the Leu at VI:16/6.51 (Leu-272) in this receptor interacts hydro-

Elucidation of $7\alpha,25$ -Dihydroxycholesterol Binding to EBI2

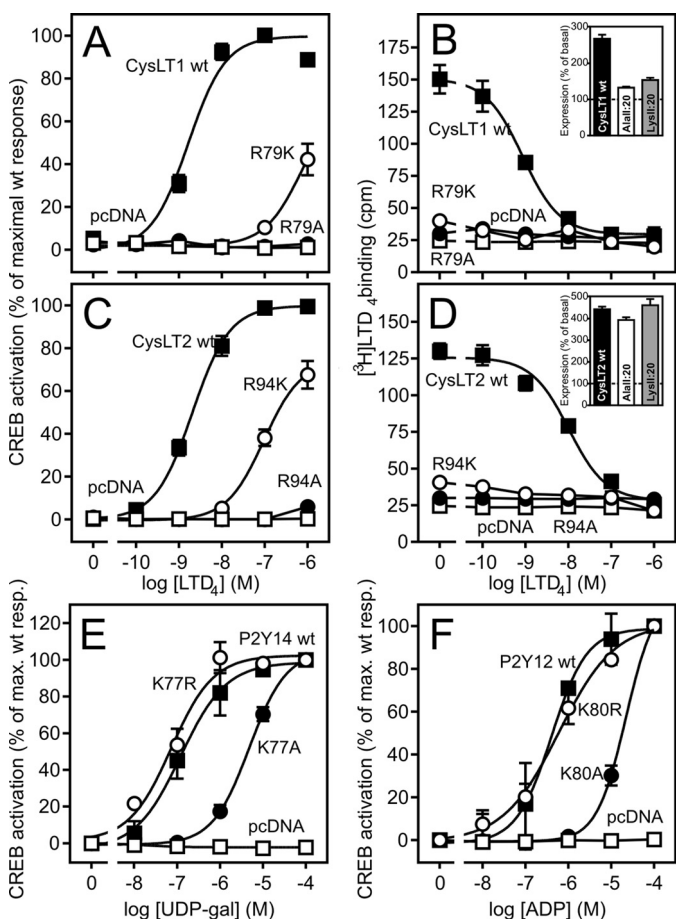


FIGURE 7. Importance of position II:20/2.60 for the CysLT receptors, P2Y12 and P2Y14. **A**, LTD₄-induced CREB activation in HEK293 cells transiently transfected with CREB-Luc reporter vector and FLAG-tagged human CysLT1 WT (solid squares), pcDNA (open squares), Ala (R79A; solid circles), or Lys (R79K; open circles) II:20/2.60 mutant. The data are normalized to the activity in pcDNA-transfected cells in the absence of LTD₄ (0%) and the maximal stimulation of CysLT1 WT by LTD₄ (100%) and are the means \pm S.E. of four independent experiments. **B**, homologous competition assay for [³H]LTD₄ binding to membranes from HEK293 cells transiently transfected with FLAG-tagged human CysLT1 WT (solid squares), pcDNA (open squares), Ala (R79A; solid circles), or Lys (R79K; open circles) II:20/2.60 mutant. The data represent means \pm S.E. of raw data from four independent experiments. *Inset*, cell surface expression of FLAG-tagged CysLT1 WT (black), Ala (R79A; white), or Lys (R79K; gray) II:20/2.60 mutants as measured by ELISA. The results are given relative to basal level in pcDNA-transfected cells (indicated by the dashed line) in percent as means \pm S.E. of three independent experiments. **C**, LTD₄-induced activation of the equivalent human CysLT2 constructs (WT receptor, Ala (R94A) or Lys (R94K) II:20/2.60 mutant). Performed and presented as in **A**. **D**, homologous competition assay for [³H]LTD₄ binding to the human CysLT2 constructs. Performed and presented as in **B**. **E**, UDP-galactose-induced CREB activation in HEK293 cells transiently transfected with CREB-Luc reporter vector, G_{q14}myr (30 ng/well), and FLAG-tagged P2Y14 WT (solid squares), pcDNA (open squares), Ala (K77A; solid circles), or Arg (K77R; open circles) II:20/2.60 mutant at 1 ng of DNA per well. The data are normalized to the activity in pcDNA-transfected cells in the absence of ADP (0%) and the maximal stimulation of P2Y12 WT by ADP (100%) and are means \pm S.E. of four independent experiments. **F**, ADP-induced CREB activation in HEK293 cells transiently transfected with CREB-Luc reporter vector, G_{q14}myr (30 ng/well), and FLAG-tagged hP2Y12 WT (solid squares), pcDNA (open squares), Ala (K80A; solid circles), or Arg (K80R; open circles) II:20/2.60 mutant. The data are normalized as in **E**.

phobically with the aliphatic portion of the sphingosine-like antagonist ML056 and, as indicated by *in silico* modeling, the agonist sphingosine 1-phosphate as well (28). We targeted several residues in TM-III and identified Tyr-112 (position III:09/3.33) and Tyr-116 (position III:13/3.37) to be important for

$7\alpha,25$ -OHC binding (Figs. 2 and 3). Of note, Phe-111 at position III:08/3.32 did not play a role for agonist binding (Table 1) although this residue is crucial for the EBI2 inverse agonist/antagonist GSK682753A (29). Although Tyr-116 presumably forms hydrogen bonds with the $7\alpha,25$ -OHC 3 β -OH group (Fig. 4), Tyr-112 likely interacts hydrophobically with the agonist steroid backbone as suggested by the WT-like binding and activation of the Y116F mutant (Fig. 3) or alternatively stabilizes Tyr-116 via π -stacking. Interestingly, a similar scenario is observed in the S1P1 receptor in which the Phe at position III:09/3.33 (Phe-125) interacts with the aliphatic portion of the sphingosine ligands (28).

Majority of Apparent EBI2 Constitutive Activity Is Likely Caused by Oxysterols Present in Medium—We identified Arg-87 at position II:20/2.60 as the third residue crucial for agonist binding (Fig. 3). We have previously shown that this residue is essential for the apparent constitutive activity of EBI2 as Arg to Ala substitution completely abolished this activity (19). However, as this substitution attenuates $7\alpha,25$ -OHC binding and receptor activation (Fig. 3), we suspect that the major part of the apparent EBI2 constitutive activity has been a consequence of agonist contamination in the medium. This is corroborated by the observation that in both transiently and stably transfected HEK293 cells (which were used in the analysis of constitutive activity), we failed to see any $7\alpha,25$ -OHC-induced activation but observed a high level of constitutive activity. On the contrary, in CHO cells, which were used in this study, we did see $7\alpha,25$ -OHC-induced activation but no constitutive activity (data not shown). Also, medium from cultured HEK293 cells has recently been shown to attract EBI2-transduced M12 cells but not controls (39). Importantly, this could be blocked by an inhibitor of the cholesterol biosynthetic pathway. Furthermore, a similar phenomenon has been reported for the free fatty acid-activated receptor GPR40 (FFAR1) in which fatty acids released from cells into the medium accounted for the apparent constitutive activity of this receptor (20). Thus, care has to be taken when choosing cell lines and interpreting constitutive activity especially in the case of lipid-activated receptors.

Top of TM-II Is Important for Ligand Binding in Several 7TM Receptors—Position II:20/2.60 has been shown to be crucial for ligand binding in a range of receptors. Of note, these are all ProII:18 or non-Pro receptors, *i.e.* position II:20/2.60 faces toward the binding pocket providing a suitable anchor point (Fig. 6). For instance, the Trp at II:20/2.60 in CXCR4 (a ProII:18 receptor) provides stabilizing hydrophobic contacts to the small molecule antagonist IT1t as evident from the recent crystal structure of this receptor (21). Similarly, the Asn at II:20/2.60 in the S1P1 receptor (a non-Pro receptor) is crucial for the binding of sphingosine-like ligands through polar contacts to the protonated primary amine in these compounds (28). In this study, we furthermore show that binding of leukotrienes to the CysLT receptors (both ProII:18 receptors) is highly dependent on the Arg at II:20/2.60 (Fig. 7). Leukotrienes contain several negatively charged and polar groups that could interact with the Arg guanidinium group. Of note, substituting the Arg with a Lys had a much more profound effect on agonist binding and receptor activation in the CysLTs (Fig. 7) compared with EBI2

(Fig. 3). This may reflect that several amines (as found in the guanidinium group) are required for agonist binding through interaction with more than one group in the ligand. In addition, the Arg at II:20/2.60 in the LPA5 receptor, another lipid-activated receptor, was shown to be functionally important as mutation of this residue completely abolished agonist-induced activation (40). This was also recently shown to be the case in GPR81 (41). Interestingly, the conservative Arg to Lys mutation also abolished receptor activation indicating a high structural specificity in this case. Although binding experiments were not performed in these two studies, it is likely that the Arg at II:20/2.60 anchors the agonists through an ionic and/or polar interaction as observed for the leukotrienes. Besides these lipid-activated receptors, we also demonstrate that the Lys at II:20/2.60 in the P2Y12 and P2Y14 receptors are important for nucleotide-induced activation in which Ala substitution results in a 50–100-fold reduction in potency (Fig. 7). In general, it is noteworthy that ProII:18 receptors that contain a positively charged residue at II:20/2.60 are mostly activated by lipids or, to a lesser extent, nucleotides (Table 2). This indicates that the positively charged II:20/2.60 residue has been conserved as an important residue for agonist binding in this subgroup of receptors.

Importance of TM-II for the 7TM Receptor Activity State in General—We also examined the role of the Asp at position II:10/2.50 (Asp-77). This residue is located three helix turns below II:20/2.60 on the same helix face. In the recent crystal structure of the activated β_2 -adrenergic receptor in complex with a G protein, the Asp at II:10 interacts with the highly conserved Asn at position VII:16 (32), whereas this interaction is absent in the inactive state (33). In line with this, Asp-77 is not required for 7 α ,25-OHC binding to EBI2 but is crucial for receptor activation thus functioning as a micro switch (Fig. 5). This is further corroborated by the D77R mutant that (contrary to D77A) still showed activation despite that the mutation introduces a charge swap. In fact, the potency is even slightly increased (4-fold) compared with the WT receptor (Fig. 5 and Table 1). Furthermore, introducing an Arg at position II:10/2.50 in the R87A mutant (which does not bind 7 α ,25-OHC, see Fig. 3A) rescued binding of the agonist (Fig. 5D). This is most likely not due to a direct interaction between 7 α ,25-OHC and the Arg at II:10/2.50 as the distance between the putative binding site and this residue is too long (~ 16 Å). A possible explanation is that the Arg substitution (in combination with R87A) induces a conformational change in EBI2 that skews the receptor population to a relatively more active (*i.e.* agonist binding) conformation. The D77R mutation has a significantly larger side chain and physicochemical properties that might repack side chains within the surrounding environment thereby moving TM-VI and/or -VII outward. Such a movement is indeed a crucial part of receptor activation (32) in which the mutation could skew the equilibrium toward an active conformation and thus favor ligand binding. For Arg-87, we only observed very few direct interactions with the agonist in our docking simulations (Fig. 4) suggesting that the interaction could be indirect, *e.g.* via water molecules. Alternatively, Arg-87 could lock EBI2 in an active conformation favoring agonist binding as observed for the II:10/2.50 mutations described above.

The importance of residues in TM-II for the activity of 7TM receptors has been observed in other rhodopsin-like 7TM receptors as well. For instance, in the neurokinin 1 (NK1) receptor, a range of mutations in TM-II facing the binding pocket affects the interchange between different receptor conformations binding either antagonists or agonists (42). Furthermore, evidence indirectly supporting the importance of this helix has been observed in several cases. For instance, introducing a positively charged residue in TM-II has been shown previously to render 7TM receptors highly constitutively active. This includes a naturally occurring mutation at position II:20/2.60 in the murine melanocortin 1 receptor (a non-Pro receptor), which substitutes the endogenous Glu with a Lys and results in a darker coat color and, importantly, abolishes agonist-induced activation (43). Of note, mutation to Arg, but not Ala or Asp, constitutively activated the receptor indicating the charge to be of importance (44, 45). Finally, a similar phenomenon was observed in the chemokine receptors CCR5 and CCR2 where introduction of Lys or Arg at position II:16/2.56 constitutively activated the receptors (46). For CCR5, this is also the case if the positively charged residue is introduced at position II:20/2.60.⁴ We speculate that introduction of Lys/Arg residues in TM-II, being centrally located in the binding pocket, may in general affect the dynamic properties and the activity of some 7TM receptors through modulation of pK_a values in surrounding residues, alternative packing of adjacent side chains, formation of new hydrogen bonding networks through water molecules or ions, and/or electrostatic interactions to ligands and ions.

In conclusion, we have mapped the binding of the most potent EBI2-activating oxysterol 7 α ,25-OHC identifying the four key residues Arg-87, Tyr-112, Tyr-116, and Tyr-260. To our knowledge, this is the first data elucidating the binding mode of an oxysterol to a 7TM receptor. Furthermore, our data suggest that position II:20/2.60 may serve as a generally important residue for ligand binding in a subgroup of 7TM receptors.

Acknowledgments—We thank Inger Smith Simonsen and Mirka Vanek for excellent technical assistance. Klaus Seuwen is thanked for support and continuous encouragement during the course of this study.

REFERENCES

- Xu, L., Bai, Q., Rodriguez-Agudo, D., Hylemon, P. B., Heuman, D. M., Pandak, W. M., and Ren, S. (2010) Regulation of hepatocyte lipid metabolism and inflammatory response by 25-hydroxycholesterol and 25-hydroxycholesterol-3-sulfate. *Lipids* **45**, 821–832
- Radhakrishnan, A., Ikeda, Y., Kwon, H. J., Brown, M. S., and Goldstein, J. L. (2007) Sterol-regulated transport of SREBPs from endoplasmic reticulum to Golgi. Oxysterols block transport by binding to Insig. *Proc. Natl. Acad. Sci. U.S.A.* **104**, 6511–6518
- Panini, S. R., Yang, L., Rusinol, A. E., Sinensky, M. S., Bonventre, J. V., and Leslie, C. C. (2001) Arachidonate metabolism and the signaling pathway of induction of apoptosis by oxidized LDL/oxysterol. *J. Lipid Res.* **42**, 1678–1686
- Rentero, C., Zech, T., Quinn, C. M., Engelhardt, K., Williamson, D., Grewal, T., Jessup, W., Harder, T., and Gaus, K. (2008) Functional implications of plasma membrane condensation for T cell activation. *PLoS One* **3**, e2262

⁴ T. Benned-Jensen, unpublished results.

Elucidation of 7 α ,25-Dihydroxycholesterol Binding to EBI2

- Janowski, B. A., Grogan, M. J., Jones, S. A., Wisely, G. B., Kliewer, S. A., Corey, E. J., and Mangelsdorf, D. J. (1999) Structural requirements of ligands for the oxysterol liver X receptors LXR α and LXR β . *Proc. Natl. Acad. Sci. U.S.A.* **96**, 266–271
- Janowski, B. A., Willy, P. J., Devi, T. R., Falck, J. R., and Mangelsdorf, D. J. (1996) An oxysterol signaling pathway mediated by the nuclear receptor LXR α . *Nature* **383**, 728–731
- Lehmann, J. M., Kliewer, S. A., Moore, L. B., Smith-Oliver, T. A., Oliver, B. B., Su, J. L., Sundseth, S. S., Winegar, D. A., Blanchard, D. E., Spencer, T. A., and Willson, T. M. (1997) Activation of the nuclear receptor LXR by oxysterols defines a new hormone response pathway. *J. Biol. Chem.* **272**, 3137–3140
- Jin, L., Martynowski, D., Zheng, S., Wada, T., Xie, W., and Li, Y. (2010) Structural basis for hydroxycholesterols as natural ligands of orphan nuclear receptor ROR γ . *Mol. Endocrinol.* **24**, 923–929
- Huh, J. R., Leung, M. W., Huang, P., Ryan, D. A., Krout, M. R., Malapaka, R. R., Chow, J., Manel, N., Ciofani, M., Kim, S. V., Cuesta, A., Santori, F. R., Lafaille, J. J., Xu, H. E., Gin, D. Y., Rastinejad, F., and Littman, D. R. (2011) Digoxin and its derivatives suppress TH17 cell differentiation by antagonizing ROR γ t activity. *Nature* **472**, 486–490
- Solt, L. A., Kumar, N., Nuhant, P., Wang, Y., Lauer, J. L., Liu, J., Istrate, M. A., Kamenecka, T. M., Roush, W. R., Vidovic, D., Schürer, S. C., Xu, J., Wagoner, G., Drew, P. D., Griffin, P. R., and Burris, T. P. (2011) Suppression of TH17 differentiation and autoimmunity by a synthetic ROR ligand. *Nature* **472**, 491–494
- Nachtergaele, S., Mydock, L. K., Krishnan, K., Rammohan, J., Schlesinger, P. H., Covey, D. F., and Rohatgi, R. (2012) Oxysterols are allosteric activators of the oncoprotein Smoothed. *Nat Chem. Biol.* **8**, 211–220
- Hannedouche, S., Zhang, J., Yi, T., Shen, W., Nguyen, D., Pereira, J. P., Guerini, D., Baumgarten, B. U., Roggo, S., Wen, B., Knochenmuss, R., Noël, S., Gessier, F., Kelly, L. M., Vanek, M., Laurent, S., Preuss, I., Miault, C., Christen, I., Karuna, R., Li, W., Koo, D. I., Suply, T., Schmedt, C., Peters, E. C., Falchetto, R., Katopodis, A., Spanka, C., Roy, M. O., Dethoux, M., Chen, Y. A., Schultz, P. G., Cho, C. Y., Seuwen, K., Cyster, J. G., and Sailer, A. W. (2011) Oxysterols direct immune cell migration via EBI2. *Nature* **475**, 524–527
- Liu, C., Yang, X. V., Wu, J., Kuei, C., Mani, N. S., Zhang, L., Yu, J., Sutton, S. W., Qin, N., Banie, H., Karlsson, L., Sun, S., and Lovenberg, T. W. (2011) Oxysterols direct B-cell migration through EBI2. *Nature* **475**, 519–523
- Rosenkilde, M. M., Benned-Jensen, T., Andersen, H., Holst, P. J., Kledal, T. N., Lüttichau, H. R., Larsen, J. K., Christensen, J. P., and Schwartz, T. W. (2006) Molecular pharmacological phenotyping of EBI2. An orphan seven-transmembrane receptor with constitutive activity. *J. Biol. Chem.* **281**, 13199–13208
- Birkenbach, M., Josefsen, K., Yalamanchili, R., Lenoir, G., and Kieff, E. (1993) Epstein-Barr virus-induced genes. First lymphocyte-specific G protein-coupled peptide receptors. *J. Virol.* **67**, 2209–2220
- Gatto, D., Paus, D., Basten, A., Mackay, C. R., and Brink, R. (2009) Guidance of B cells by the orphan G protein-coupled receptor EBI2 shapes humoral immune responses. *Immunity* **31**, 259–269
- Pereira, J. P., Kelly, L. M., Xu, Y., and Cyster, J. G. (2009) EBI2 mediates B cell segregation between the outer and center follicle. *Nature* **460**, 1122–1126
- Im, Y. J., Raychaudhuri, S., Prinz, W. A., and Hurley, J. H. (2005) Structural mechanism for sterol sensing and transport by OSBP-related proteins. *Nature* **437**, 154–158
- Benned-Jensen, T., and Rosenkilde, M. M. (2008) Structural motifs of importance for the constitutive activity of the orphan 7TM receptor EBI2. Analysis of receptor activation in the absence of an agonist. *Mol. Pharmacol.* **74**, 1008–1021
- Stoddart, L. A., Brown, A. J., and Milligan, G. (2007) Uncovering the pharmacology of the G protein-coupled receptor GPR40. High apparent constitutive activity in guanosine 5'-O-(3-[³⁵S]thio)triphosphate binding studies reflects binding of an endogenous agonist. *Mol. Pharmacol.* **71**, 994–1005
- Wu, B., Chien, E. Y., Mol, C. D., Fenalti, G., Liu, W., Katritch, V., Abagyan, R., Brooun, A., Wells, P., Bi, F. C., Hamel, D. J., Kuhn, P., Handel, T. M., Cherezov, V., and Stevens, R. C. (2010) Structures of the CXCR4 chemokine GPCR with small molecule and cyclic peptide antagonists. *Science* **330**, 1066–1071
- Barth, P., Schonbrun, J., and Baker, D. (2007) Toward high resolution prediction and design of transmembrane helical protein structures. *Proc. Natl. Acad. Sci. U.S.A.* **104**, 15682–15687
- Leaver-Fay, A., Tyka, M., Lewis, S. M., Lange, O. F., Thompson, J., Jacak, R., Kaufman, K., Renfrew, P. D., Smith, C. A., Sheffler, W., Davis, I. W., Cooper, S., Treuille, A., Mandell, D. J., Richter, F., Ban, Y. E., Fleishman, S. J., Corn, J. E., Kim, D. E., Lyskov, S., Berrondo, M., Mentzer, S., Popović, Z., Havranek, J. J., Karanicolas, J., Das, R., Meiler, J., Kortemme, T., Gray, J. J., Kuhlman, B., Baker, D., and Bradley, P. (2011) ROSETTA3. An object-oriented software suite for the simulation and design of macromolecules. *Methods Enzymol.* **487**, 545–574
- Meiler, J., and Baker, D. (2006) ROSETTALIGAND. Protein-small molecule docking with full side-chain flexibility. *Proteins* **65**, 538–548
- Lemmon, G., and Meiler, J. (2012) Rosetta ligand docking with flexible XML protocols. *Methods. Mol. Biol.* **819**, 143–155
- Shindyalov, I. N., and Bourne, P. E. (1998) Protein structure alignment by incremental combinatorial extension (CE) of the optimal path. *Protein. Eng.* **11**, 739–747
- Alexander, N., Woetzel, N., and Meiler, J. (2011) 2011 IEEE 1st International Conference on Computational Advances in Bio and Medical Sciences (ICCBS) Orlando, Florida, February 3–5, 2011, pp. 13–18, IEEE Computer Society, Washington, D. C.
- Hanson, M. A., Roth, C. B., Jo, E., Griffith, M. T., Scott, F. L., Reinhart, G., Desale, H., Clemons, B., Cahalan, S. M., Schuerer, S. C., Sanna, M. G., Han, G. W., Kuhn, P., Rosen, H., and Stevens, R. C. (2012) Crystal structure of a lipid G protein-coupled receptor. *Science* **335**, 851–855
- Benned-Jensen, T., Smethurst, C., Holst, P. J., Page, K. R., Sauls, H., Sivertsen, B., Schwartz, T. W., Blanchard, A., Jepras, R., and Rosenkilde, M. M. (2011) Ligand modulation of the Epstein-Barr virus-induced seven-transmembrane receptor EBI2. Identification of a potent and efficacious inverse agonist. *J. Biol. Chem.* **286**, 29292–29302
- Rosenkilde, M. M., Benned-Jensen, T., Frimurer, T. M., and Schwartz, T. W. (2010) The minor binding pocket. A major player in 7TM receptor activation. *Trends Pharmacol. Sci.* **31**, 567–574
- Warne, T., Serrano-Vega, M. J., Baker, J. G., Moukhametzianov, R., Edwards, P. C., Henderson, R., Leslie, A. G., Tate, C. G., and Schertler, G. F. (2008) Structure of a β_1 -adrenergic G-protein-coupled receptor. *Nature* **454**, 486–491
- Rasmussen, S. G., DeVree, B. T., Zou, Y., Kruse, A. C., Chung, K. Y., Kobilka, T. S., Thian, F. S., Chae, P. S., Pardon, E., Calinski, D., Mathiesen, J. M., Shah, S. T., Lyons, J. A., Caffrey, M., Gellman, S. H., Steyaert, J., Skiniotis, G., Weis, W. I., Sunahara, R. K., and Kobilka, B. K. (2011) Crystal structure of the β_2 -adrenergic receptor-G_s protein complex. *Nature* **477**, 549–555
- Cherezov, V., Rosenbaum, D. M., Hanson, M. A., Rasmussen, S. G., Thian, F. S., Kobilka, T. S., Choi, H. J., Kuhn, P., Weis, W. I., Kobilka, B. K., and Stevens, R. C. (2007) High resolution crystal structure of an engineered human β_2 -adrenergic G protein-coupled receptor. *Science* **318**, 1258–1265
- Altenbach, C., Kusnetzow, A. K., Ernst, O. P., Hofmann, K. P., and Hubbell, W. L. (2008) High resolution distance mapping in rhodopsin reveals the pattern of helix movement due to activation. *Proc. Natl. Acad. Sci. U.S.A.* **105**, 7439–7444
- Holst, B., Frimurer, T. M., Mokrosinski, J., Halkjaer, T., Cullberg, K. B., Underwood, C. R., and Schwartz, T. W. (2009) Overlapping binding site for the endogenous agonist, small molecule agonists, and ago-allosteric modulators on the ghrelin receptor. *Mol. Pharmacol.* **75**, 44–59
- Holst, B., Holliday, N. D., Bach, A., Elling, C. E., Cox, H. M., and Schwartz, T. W. (2004) Common structural basis for constitutive activity of the ghrelin receptor family. *J. Biol. Chem.* **279**, 53806–53817
- Elling, C. E., Frimurer, T. M., Gerlach, L. O., Jorgensen, R., Holst, B., and Schwartz, T. W. (2006) Metal ion site engineering indicates a global toggle switch model for seven-transmembrane receptor activation. *J. Biol. Chem.* **281**, 17337–17346
- Rosenkilde, M. M., Andersen, M. B., Nygaard, R., Frimurer, T. M., and Schwartz, T. W. (2007) Activation of the CXCR3 chemokine receptor through anchoring of a small molecule chelator ligand between TM-III, -IV, and -VI. *Mol. Pharmacol.* **71**, 930–941

39. Kelly, L. M., Pereira, J. P., Yi, T., Xu, Y., and Cyster, J. G. (2011) EBI2 guides serial movements of activated B cells and ligand activity is detectable in lymphoid and nonlymphoid tissues. *J. Immunol.* **187**, 3026–3032
40. Williams, J. R., Khandoga, A. L., Goyal, P., Fells, J. I., Perygin, D. H., Siess, W., Parrill, A. L., Tigyi, G., and Fujiwara, Y. (2009) Unique ligand selectivity of the GPR92/LPA5 lysophosphatidate receptor indicates role in human platelet activation. *J. Biol. Chem.* **284**, 17304–17319
41. Kuei, C., Yu, J., Zhu, J., Wu, J., Zhang, L., Shih, A., Mirzadegan, T., Lovenberg, T., and Liu, C. (2011) Study of GPR81, the lactate receptor, from distant species identifies residues and motifs critical for GPR81 functions. *Mol. Pharmacol.* **80**, 848–858
42. Rosenkilde, M. M., Cahir, M., Gether, U., Hjorth, S. A., and Schwartz, T. W. (1994) Mutations along transmembrane segment II of the NK-1 receptor affect substance P competition with non-peptide antagonists but not substance P binding. *J. Biol. Chem.* **269**, 28160–28164
43. Robbins, L. S., Nadeau, J. H., Johnson, K. R., Kelly, M. A., Roselli-Rehffuss, L., Baack, E., Mountjoy, K. G., and Cone, R. D. (1993) Pigmentation phenotypes of variant extension locus alleles result from point mutations that alter MSH receptor function. *Cell* **72**, 827–834
44. Benned-Jensen, T., Mokrosinski, J., and Rosenkilde, M. M. (2011) The E92K melanocortin 1 receptor mutant induces cAMP production and arrestin recruitment but not ERK activity indicating biased constitutive signaling. *PLoS One* **6**, e24644
45. Lu, D., Vage, D. I., and Cone, R. D. (1998) A ligand-mimetic model for constitutive activation of the melanocortin-1 receptor. *Mol. Endocrinol.* **12**, 592–604
46. Alvarez Arias, D., Navenot, J. M., Zhang, W. B., Broach, J., and Peiper, S. C. (2003) Constitutive activation of CCR5 and CCR2 induced by conformational changes in the conserved TXP motif in transmembrane helix 2. *J. Biol. Chem.* **278**, 36513–36521